



Anisotropic electrical and dispersive optical parameters in InS layered crystals

A.F. Qasrawi^{a,b,*}, N.M. Gasanly^c

^a Group of Physics, Faculty of Engineering, Atilim University, 06836 Ankara, Turkey

^b Department of Physics, Arab-American University, Jenin, West Bank, Palestine

^c Department of Physics, Middle East Technical University, 06531 Ankara, Turkey

ARTICLE INFO

Article history:

Received 5 September 2009

Received in revised form

14 October 2009

Accepted 16 November 2009

by R. Phillips

Available online 22 November 2009

Keywords:

A. Semiconductors

B. Crystal growth

D. Electronic transport

D. Optical properties

ABSTRACT

The anisotropy effect on the current transport mechanism and on the dispersive optical parameters of indium monosulfide crystals has been studied by means of electrical conductivity and polarized reflectance measurements along the *a*-axis and the *b*-axis, respectively. The temperature-dependent electrical conductivity analysis in the range 10–350 K for the *a*-axis and in the range 30–350 K for the *b*-axis revealed the domination of the thermionic emission of charge carriers and the domination of variable range hopping above and below 100 K, respectively. At high temperatures ($T > 100$ K) the conductivity anisotropy, s , decreased sharply with decreasing temperature following the law $s \propto \exp(-E_s/kT)$. The anisotropy activation energy, E_s , was found to be 330 and 17 meV above and below 220 K, respectively. Below 100 K, the conductivity anisotropy is invariant with temperature. In that region, the calculated hopping parameters are altered significantly by the conductivity anisotropy. The optical reflectivity analysis in the wavelength range 250–650 nm revealed a clear anisotropy effect on the dispersive optical parameters. In particular, the static refractive index, static dielectric constant, lattice dielectric constant, dispersion energy and oscillator energy exhibited values of 2.89, 8.39, 19.7, 30.02 eV and 4.06 eV, and values of 2.76, 7.64, 25.9, 22.26 eV and 3.35 eV for light polarized along the *a*-axis and the *b*-axis, respectively.

© 2009 Elsevier Ltd. All rights reserved.

1. Introduction

Recently, In_xS_y -type semiconductors have attracted much attention due to their wide applications in technology. For example, In_2S_3 is reported to have several important applications in dry cells [1], color televisions [2–4] and photovoltaic electric generators [5,6]. In_2S_3 nanoparticle bio-conjugates are also stated to have medical applications for cancer diagnosis [7]. Furthermore, indium sulfide is being used as buffering material for $\text{Cu}(\text{In}, \text{Ga})\text{Se}_2$ -based solar cells [8]. In addition, In_6S_7 is also reported to have good photovoltaic properties. The maximum open-circuit voltage and short-circuit photocurrent density, which are related to an illumination intensity equivalent to one sun, are reported as 0.12 V and 0.38 mA cm^{-2} , respectively, for this crystal [9].

Previously, we have studied the carrier transport and the optoelectronic properties of InS single crystals [10,11]. In particular, the donor level energies, the carrier effective mass, the carrier compensation ratio and the acoustic deformation potential for

this crystal were estimated [10]. In addition, the optoelectronic and electric properties, studied along the *a*-axis of the crystal, have shown that the spectral distribution of photocurrent in the photon energy range 0.8–3.1 eV reveals an indirect band gap of 1.91 eV [11]. The photocurrent–illumination intensity dependence was reported to follow the law $I_{\text{ph}} \propto F^\gamma$, with γ being 1.0 and 0.5 at low and high illumination intensities, indicating the domination of monomolecular and bimolecular recombination, respectively.

In the current study we will concentrate on the anisotropy effects on the electrical and optical properties of InS single crystals. In other words, we are going to report the anisotropy effect on the dominant transport mechanism and on the dispersive optical parameters along the *a*-axis and the *b*-axis of the crystal. In particular, the donor states, the Mott variable range hopping parameters and the static and lattice dielectric constants as well as the oscillator energy, the dispersion energy and the static refractive index along both axes will be calculated, compared and discussed.

2. Experimental details

Indium sulfide polycrystals were synthesized from high-purity elements (at least 99.999%) taken in stoichiometric proportions. Single crystals of InS were grown by the Bridgman method. The analysis of X-ray diffraction data revealed that they crystallize

* Corresponding author at: Group of Physics, Faculty of Engineering, Atilim University, 06836 Ankara, Turkey. Tel.: +90 312 5868329; fax: +90 312 5868091.

E-mail address: atef.qasrawi@atilim.edu.tr (A.F. Qasrawi).

in an orthorhombic unit cell with parameters $a = 0.394$, $b = 0.444$ and $c = 1.065$ nm. Due to the fact that one of the three In–S bonds extends into neighboring layers, InS crystals have no distinct cleavage plane. Crystals suitable for measurements were obtained by hard cleavage along (001) planes, perpendicular to the c -axis. Typical dimensions of the van der Pauw samples were $3 \times 3 \times 1$ mm³. Ohmic contacts for the electrical measurements were made using high-purity indium. The temperature-dependent dark electrical conductivity measurements were carried out in the temperature range 10–350 K in an automated closed-cycle Lakeshore cryogenic system.

3. Results and discussion

The dark electrical conductivity measurements were carried out along the a -axis and the b -axis of the crystal in the temperature ranges 10–350 K and 30–350 K, respectively. The data are displayed in Fig. 1(a). As is clear from the figure and its inset, except for a critical temperature of 270 K, the values of the electrical conductivity along the a -axis and the b -axis exhibit different numerical values at each temperature. The lower the temperature, the larger the conductivity values difference. This behavior is an indication of temperature-dependent crystal anisotropy. The electrical anisotropy (s) defined by the relative conductivity ratio, σ_b/σ_a , is illustrated in Fig. 1(b). As is evident from this figure, the anisotropy of InS crystals at 350 K is 23.1; it decreases sharply to 3.8 at 300 K and reaches 0.05 at 200 K. Below 200 K, the conductivity ratio continues decreasing, but with a different trend down to 100 K. Below this temperature the anisotropy tends to remain constant with temperature. The conductivity anisotropy was also observed in TlSe [12,13] and InTe [14,15] crystals and was attributed to: (i) the high concentration of stacking faults due to weak interchain bonding [14]; here, the conductivity anisotropy is proportional to the inverse square of the overlap energy associated with the bonding between adjacent chains; and (ii) the high anisotropy of the direction-dependent effective masses in the crystal [15].

To reveal the anisotropy effect on the dominant transport mechanisms in InS crystals, the conductivity–temperature dependence was analyzed according to the thermionic emission of charged carriers [16] in which the conductivity was represented by the relation $\sigma = Lq^2p\sqrt{1/(2\pi m^*kT)} \exp(-E_\sigma/kT)$. Here L is the grain size, q is the electronic charge, p is the carrier concentration, m^* is the carrier effective mass and E_σ is the conductivity activation energy. This equation can be rewritten as $\sigma\sqrt{T} = \sigma_0 \exp(-E_\sigma/kT)$, with $\sigma_0 = Lq^2p(2\pi m^*k)^{-1/2}$. As shown in Fig. 1(a), calculations of the conductivity activation energy along the a -axis and the b -axis in the temperature ranges 10–350 K and 30–350 K revealed values of 164, 50 and 10 meV, and 500, 37 and 10 meV in the temperature ranges 220–350, 110–210 and 10–100 K, and 210–350, 110–200 and 30–100 K, respectively. The origin of these energy states was previously discussed and assigned to the impurity carriers being located at different energy levels below the conduction band [10,11].

Since the conductivity in both directions satisfies the same equation, the anisotropy in the conductivity can be represented by

$$s = \frac{\sigma_b}{\sigma_a} = \sigma_1 \exp(-(E_{\sigma b} - E_{\sigma a})/kT) = \sigma_1 \exp(-E_s/kT). \quad (1)$$

Here, σ_1 and E_s are the pre-exponential factor and the anisotropy activation energy, respectively. The values of E_s , calculated from the slope of the $\ln(s) - T^{-1}$ plot (Fig. 1(b)), are found to be ~ 330 meV above 220 K and ~ 17 meV in the moderate-temperature region. In the low-temperature regions (10–100 K for the a -axis and 30–100 K for the b -axis), the invariance of the conductivity anisotropy and the very low value of the activation energy

Table 1
Anisotropic electrical and dispersive optical parameters in InS crystals.

	Parameter	a -axis	b -axis
Electrical	E_σ (meV)		
	$T \geq 220$ K	164	500
	$110 \leq T \leq 210$ K	50	37
	$T \leq 100$ K	10	10
	T_0 ($\times 10^6$ K)	3.85	2.83
	γ (cm ⁻¹)	1.03×10^7	7.95×10^4
	$N(E_F)$ (cm ⁻³ eV ⁻¹)	5.91×10^{19}	3.70×10^{13}
	R (70 K) (cm)	5.59×10^{-7}	6.70×10^{-5}
	W (70 K) (meV)	23.15	21.43
γR	5.75	5.33	
Optical	E_1 (eV)	30.02	22.26
	E_0 (eV)	4.06	3.35
	n_0	2.89	2.76
	ε_s	8.39	7.64
	ε_L	19.70	25.91

(~ 10 meV) reflect the possibility of the domination of another transport mechanism in this region of temperatures.

The $\sigma - T$ data in the temperature ranges 10–100 K (for the a -axis) and 30–100 K (for the b -axis) were best explained with the Mott variable range hopping mechanism [17,18], in which the expression for the conductivity at low temperatures is given by

$$\sigma\sqrt{T} = \sigma_2 \exp\left(-\left(\frac{T_0}{T}\right)^{1/4}\right), \quad (2)$$

$$\text{where } \sigma_2 = e^2 a^2 \nu_{\text{ph}} N(E_F) \quad (3)$$

$$\text{and } T_0 = \frac{\lambda \gamma^3}{kN(E_F)}. \quad (4)$$

Here, a is the hopping distance and $\nu_{\text{ph}} = 2.56 \times 10^{13}$ s⁻¹ is the phonon frequency calculated from the Debye temperature of the crystal. λ is a dimensionless parameter (~ 18.1), $N(E_F)$ is the density of localized states near the Fermi level and γ is the decay constant. Two other parameters, R and W , the average hopping distance and the average hopping energy, respectively, are also given as

$$R = \left(\frac{9}{8\pi\gamma kTN(E_F)}\right)^{1/4} \quad (5)$$

$$\text{and } W = \frac{3}{4\pi R^3 N(E_F)}. \quad (6)$$

The linear $\ln(\sigma\sqrt{T}) - T^{-1/4}$ plots are illustrated in the inset of Fig. 1(b). Mott parameters have been calculated using Eqs. (2)–(6) and were found to satisfy Mott's requirements ($\gamma R > 1$ and $W > kT$, $T_0 > 10^3$ K) for variable range hopping to dominate (Table 1). Thus, in the low-temperature regions, thermally assisted variable range hopping conduction is the most likely transport mechanism in InS crystals. The atomic disorder degree in the crystal (defined as T_0/T) is found to be 4.81×10^4 and 3.54×10^4 at 80 K for the a -axis and the b -axis measurements, respectively. The data in the Table 1 reflect the effect of anisotropy on the variable range hopping parameters. The calculated density of localized states exhibited larger values for the conductivity being measured along the a -axis than for that being measured along the b -axis. This difference might be attributed to the deep potential barriers created at the chain boundaries.

The change in the transport mechanism from thermionic emission to variable range hopping may have occurred due to the existence of structural constraints upon electron transfer between the In–In bonds. This bond lies in the (100) plane and is inclined to the b -axis by 23.4° from the c -axis. That is, the

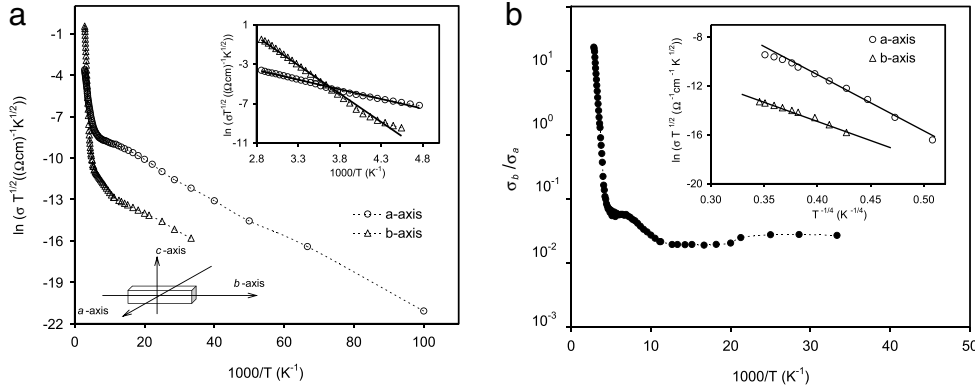


Fig. 1. (a) The $\ln(\sigma\sqrt{T}) - T^{-1}$ variation for InS crystals. The inset represents an enlargement for the high-temperature region. (b) σ_b/σ_a versus T^{-1} . The inset reflects the hopping conduction.

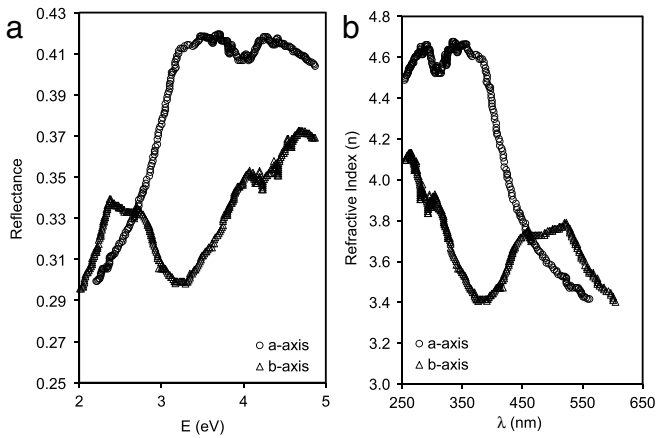


Fig. 2. (a) The optical reflectance for InS crystals as recorded by Takarabe et al. [20]. (b) The calculated refractive index as a function of wavelength.

In-In bonding direction is perpendicular to the *a*-axis. For this reason, in contrast to the *a*-axis, the transfer from In-In bonding to anti-bonding states has non-vanishing components of electric field along the *b*-axis [19]. Such types of structure usually result in a high degree of structural disorder which most probably increases the density of localized states near the Fermi level, causing the domination of the hopping mechanism.

Fig. 2(a) reflects the optical reflectance spectra measured by Takarabe et al. [20]. The displayed data relate to *a*-axis and *b*-axis polarization reflections in the incident photon energy range 2.0–5.0 eV. During their experiment, the light falls parallel to the *c*-axis with polarization of light along the *a*-axis or the *b*-axis. The authors of Ref. [20] have studied the optical absorption coefficient (α) for both polarizations. Their study revealed a stronger absorption for *a*-axis polarization than that for *b*-axis polarization. They have also revealed that the lowest direct gap of an InS crystal is allowed only for *b*-axis polarization and is forbidden for *a*-axis polarization. Further, the authors have analyzed the reflectance data to obtain an idea about the optical activity. From the latter study they have stated that in the range 2.0–3.2 eV InS is optically active for *b*-axis polarization and in the range higher than 3.2 eV it is optically active for *a*-axis polarization. Such behavior was attributed to the In-In bond location in the (100) plane inclined to the *b*-axis and perpendicular to the *a*-axis.

Following their work and using their data displayed in Fig. 9(b) of Ref. [20] and in Fig. 2(a) in this article, we have estimated the values of refractive index as a function of wavelength to carry out a single-effective-oscillator parametric analysis on the crystal. The refractive index displayed in Fig. 2(b) was estimated from a relation

in which the reflectance (*R*), the extinction coefficient (*K*) and the refractive index (*n*) of crystalline solids at a certain constant wavelength (λ) are related through the two equations [21]

$$K = \frac{\alpha\lambda}{4\pi}, \tag{7}$$

$$R = \frac{(n-1)^2 + K^2}{(n+1)^2 + K^2}. \tag{8}$$

Using these relations, the values of *K* and *n* were calculated from the measured data of *R* and α . The data for the refractive index as a function of incident wavelength are displayed in Fig. 2(b). As can be seen from Fig. 2(b), the refractive index decreases sharply with increasing wavelength (decreasing photon energy) from 388 nm (3.20 eV) down to 558 nm (2.22 eV) for *a*-axis polarization and from 261 nm (4.75 eV) down to 388 nm (3.20 eV) for *b*-axis polarization. Below 388 nm the refractive index for *b*-axis polarization increases with decreasing wavelength up to a critical wavelength value of 461 nm (2.69 eV). Below this value it tends to remain constant, with very slight increment, and at a wavelength of 520 nm (2.38 eV) it decreases sharply in a trend similar to that of *a*-axis polarization but with different numerical values.

In the transparent region ($2.00 < E < 2.38$ eV for *b*-axis polarization and $2.22 < E < 2.70$ eV for *a*-axis polarization), the data for the dispersive refractive index, $n(\lambda)$, may be analyzed using the single-effective-oscillator model [22]. This model is widely used for analyzing the refractive index of crystalline materials like ZnSe, GaAs, CdTe and ZnTe [22]. The model suggests that the data could be described by

$$n^2(E) = 1 + \frac{E_1 E_0}{E_0^2 - E^2}, \tag{9}$$

where E_1 is the dispersion energy and E_0 is the oscillator energy. Plotting $(n^2 - 1)^{-1}$ as function of E^2 allows the determination of the oscillator parameters, by fitting a linear function. The fitting of the above reported function is illustrated in Fig. 3(a). The static refractive index, $n(0)$, is evaluated from Eq. (9), i.e., $n^2(0) = 1 + E_1/E_0$. In addition, the relation between the lattice dielectric constant (ϵ_L) and the refractive index (*n*) is also given by [23]

$$n^2 = \epsilon_L - A\lambda^2, \tag{10}$$

where *A* is a constant which depends on the ratio of the carrier concentration to effective mass.

The values of E_1 and E_0 , calculated from the slope and the intersection of the straight line in Fig. 3(a), are found to be 30.02 and 4.06 eV for light polarization along the *a*-axis and 22.26 and 3.35 for light polarization along the *b*-axis, respectively. The values of the static dielectric constant, $\epsilon_s = n^2(0)$, and the static refractive

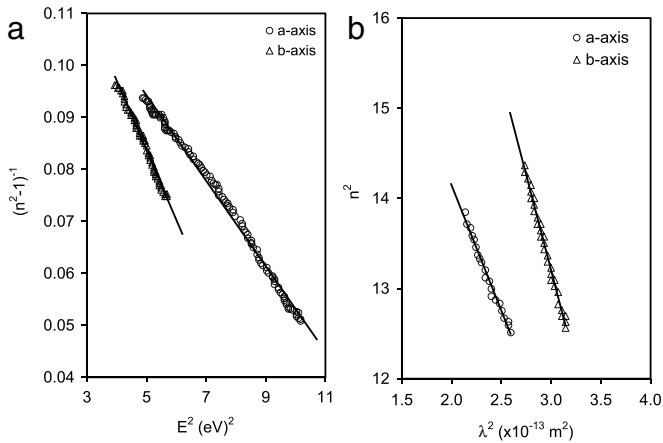


Fig. 3. (a) The $(n^2 - 1)^{-1} - E^2$ variation for InS crystals. (b) The $n^2 - \lambda^2$ variation.

index, $n(0)$, are also calculated using Eq. (9) and found to be 8.39 and 2.89 for a -axis polarization and 7.64 and 2.76 for b -axis polarization, respectively. The $n^2 - \lambda^2$ plot shown in Fig. 3(b) is also linear, verifying Eq. (10). The values of $\varepsilon_L = 19.70$ and 25.91 are also determined from the intercepts of the slopes (shown by the solid lines in Fig. 3(b)) of the $n^2 - \lambda^2$ plots. The disagreement between the values of the static and lattice dielectric constants may be attributed to the free carrier contribution [23,24]. The data obtained from the single-oscillator model are also displayed in Table 1.

4. Conclusions

In this work, anisotropy effects on the electrical and optical properties of InS single crystals were investigated. Namely, the electrical conductivity and polarized reflectance along the a -axis and the b -axis of the crystal were analyzed. The electrical data were interpreted using the thermionic emission and variable range hopping of charged carrier theories. It is concluded that the thermionic emission and the thermally assisted Mott variable range hopping of charged carriers are the dominant

transport mechanisms at high and moderate temperatures, and low temperatures, respectively. The data analysis allowed the determination of the conductivity activation energies, the density of localized states near the Fermi level, the average hopping energies and the average hopping distances in addition to the disorder degrees in the crystals. The optical data analysis has reflected a significant anisotropy effect on the dispersive optical parameters. All the dispersive optical parameters are observed to be strongly affected by the crystal anisotropy.

References

- [1] Jpn. Patent Application, Chem. Abstr. 96 (1979) 113316h.
- [2] Jpn. Patent Application, Chem. Abstr. 91 (1979) 67384a.
- [3] E. Dalas, L. Kobotiatis, J. Mater. Sci. 28 (1993) 6595.
- [4] Jpn. Patent Application, Chem. Abstr. 95 (1981) 107324x.
- [5] E. Dalas, S. Sakkopoulos, E. Vitoratos, G. Maroulis, L. Kobotiatis, J. Mater. Sci. 28 (1993) 5456.
- [6] S. Gorai, S. Chaudhuri, Mater. Sci. Eng. B 126 (2006) 97–101.
- [7] D.K. Nagesha, X. Liang, A.A. Mamedov, G. Gainer, M.A. Eastman, M. Giersig, J.J. Song, T. Ni, N.A. Kotov, J. Phys. Chem. B 105 (2001) 7490.
- [8] N. Barreau, Sol. Energy 83 (2009) 363–371.
- [9] A.F. Qasrawi, N.M. Gasanly, J. Phys.: Condens. Matter. 18 (2006) 4609–4614.
- [10] A.F. Qasrawi, N.M. Gasanly, Cryst. Res. Technol. 37 (2002) 1104–1112.
- [11] A.F. Qasrawi, N.M. Gasanly, Semicond. Sci. Technol. 17 (2002) 1288–1292.
- [12] K.R. Allakhverdiev, Sh.G. Gasymov, T.G. Mamedov, M.A. Nizametdinova, E.Yu. Salaev, Sov. Phys. Semicond. 17 (1983) 131.
- [13] A.M. Panich, J. Phys.: Condens. Matter. 20 (2008) 293202.
- [14] M. Parlak, C. Ercelebi, I. Gunal, H. Ozkan, N.M. Gasanly, Cryst. Res. Technol. 31 (1996) 673.
- [15] V. Riede, H. Neumann, H. Sobotta, Solid State Commun. 38 (1981) 71.
- [16] J.Y. Seto, J. Appl. Phys. 46 (1975) 5247.
- [17] N.F. Mott, E.A. Davis, Electronic Process in Non Crystalline Materials, Oxford, Clarendon, 1979.
- [18] D.K. Paul, S.S. Mitra, Phys. Rev. Lett. 31 (1973) 1000.
- [19] T. Takarabe, T. Nishino, J. Phys. Chem. Solids 44 (1983) 681–684.
- [20] K. Takarabe, H. Kawamura, K. Wakamura, Phys. Status Solidi (b) 142 (1987) 605–615.
- [21] J.I. Pankove, Optical Processes in Semiconductors, Prentice-Hall, New Jersey, 1971.
- [22] S.H. Wemple, M. Di Domenico, Phys. Rev. B 3 (1971) 1338.
- [23] M.M. El-Nahass, A.A.M. Farag, E.M. Ibrahim, S. Abd-El-Rahman, Vacuum 72 (2004) 453.
- [24] I.M. Ismailov, E.M. Kurbanov, Sov. Phys. J. 32 (1989) 21–25.